Title

Mechanisms of shear strain accumulation in laboratory experiments on sands exhibiting cyclic mobility behavior

Journal

Canadian Geotechnical Journal, 59(8)

ISSN

0008-3674

Authors

Humire, Francisco
Ziotopoulou, Katerina

Publication Date

2022-08-01

DOI

10.1139/cgj-2021-0373

Peer reviewed

Canadian Science Publishing

ARTICLE

Mechanisms of shear strain accumulation in laboratory experiments on sands exhibiting cyclic mobility behavior

Francisco Humire and Katerina Ziotopoulou

Abstract: The factors and mechanisms controlling the accumulation of shear strains of clean uniform sands exhibiting cyclic mobility behavior under level-ground conditions are examined. This phenomenon is investigated through a series of constant-volume cyclic direct simple shear (DSS) tests subjected to uniform and irregular loading conditions, and undrained cyclic element tests collected from the literature. Experimental data show that the rate of shear strain accumulation per loading cycle depends on the relative density, cyclic stress amplitude, and effective overburden stress. Mechanisms of shear strain accumulation are investigated by decoupling the shear strain developed in each loading cycle in two components: γ_0, developed at near-zero effective stress, and γ_d, developed during dilation. Results show that γ_0 mostly depends on the shear strain history, while γ_d depends on the cyclic stress amplitude and relative density. These dependencies of γ_d and γ_0 are used to provide an explanation for the gradual decrease of the rate of shear strain accumulation that is observed while increasing the number of post-triggering loading cycles in tests performed on dense specimens.

Key words: cyclic mobility, shear strain accumulation, liquefaction, post-triggering response, direct simple shear testing.

Résumé : Les facteurs et les mécanismes contrôlant l'accumulation des déformations de cisaillement des sables propres et homogènes présentant un comportement de mobilité cyclique dans des conditions de terrain plat sont examinés. Ce phénomène est étudié au moyen d'une série d'essais cycliques de cisaillement simple direct (DSS) à volume constant soumis à des conditions de chargement uniformes et irrégulières, et d'essais cycliques par éléments non drainés recueillis dans la littérature. Les données expérimentales montrent que le taux d'accumulation de la déformation de cisaillement par cycle de chargement dépend de la densité relative, de l'amplitude de la contrainte cyclique et de la contrainte effective de recouvrement. Les mécanismes d'accumulation de la déformation en cisaillement sont étudiés en découplant la déformation en cisaillement développée dans chaque cycle de chargement en deux composantes: γ_0, développée à une contrainte effective proche de zéro, et γ_d, développée pendant la dilatation. Les résultats montrent que γ_0 dépend principalement de l'historique des déformations de cisaillement, tandis que γ_d dépend de l'amplitude des contraintes cycliques et de la densité relative. Ces dépendances de γ_d et γ_0 sont utilisées pour fournir une explication à la diminution progressive du taux d'accumulation de la déformation de cisaillement qui est observée tout en augmentant le nombre de cycles de chargement post-déclenchement dans les essais réalisés sur des spécimens denses. [Traduit par la Rédaction]

Mots-clés : mobilité cyclique, accumulation de déformations de cisaillement, liquéfaction, réponse post-déclenchement, essai de cisaillement simple direct.

1. Introduction

Lateral deformations developed when soils exhibit cyclic mobility behavior, wherein soil progressively accumulates shear strains after liquefaction triggering, can result in significant damages to structures built on or in liquefiable sandy soils. In the context of performance-based evaluations, more reliable estimations of liquefaction-induced shear deformations are needed for the seismic design of geosystems. Progress towards more reliable estimations of such deformations in boundary value problems has been possible through the development of constitutive models capable of capturing the cyclic mobility response at the element level (e.g., Beaty and Byrne 1998; Boulanger and Ziotopoulou 2017; Khosravifar et al. 2018). Even though such constitutive models can replicate the process of shear strain accumulation, there is a very limited development of physics-based frameworks or empirical/semi-empirical correlations to guide their calibration and to better constrain predicted liquefaction-induced deformations. This is due to the lack of a fundamental understanding of the physical mechanisms and factors controlling the process of shear strain accumulation associated with the scarcity of experimental data that can serve as a baseline to guide such developments. As such, and before upscaling the problem to the system level and accounting for the uncertainties of the field (e.g., boundary conditions, spatial variability of soils), it is key to understand element-level mechanisms and the factors that control the process of shear strain accumulation.

The cyclic mobility response of sands in stress-controlled element experiments is initially characterized by a gradual decrease in the effective vertical stresses (Fig. 1*a*), followed by a progressive accumulation of limited shear strains in each loading cycle (Fig. 1*b*). In this work, triggering is defined as the soil reaching 6% double-amplitude shear strain. From that point onward, the post-triggering shear strain accumulation is typically assessed by tracking the

Received 17 August 2021. Accepted 28 January 2022.

F. Humire and K. Ziotopoulou.* Department of Civil and Environmental Engineering, University of California, Davis, CA, USA.

Corresponding author: Katerina Ziotopoulou (email: kziotopoulou@ucdavis.edu).

*Katerina Ziotopoulou served as an Editorial Board Member at the time of manuscript review and acceptance; peer review and editorial decisions regarding this manuscript were handled by Dharma Wijewickreme.

Fig. 1. Results of a constant-volume (equivalent undrained) cyclic DSS test performed on a medium-dense specimen of Ottawa F-65 sand with relative density D_R = 61.3%: (*a*) stress–strain response, (*b*) effective stress path, (*c*) shear strain accumulation per loading cycle, and (*d*) evolution of single- and double-amplitude shear strains (γ_{SA} and γ_{DA}) per loading cycle, and definition of post-triggering shear strains ($\gamma_{post\text{-}trigg}$) and post-triggering cycles ($N_{post\text{-}trigg}$). Superscripts + and − indicate the single amplitude shear strain accumulated in the positive and negative loading directions, respectively. [Color online.]

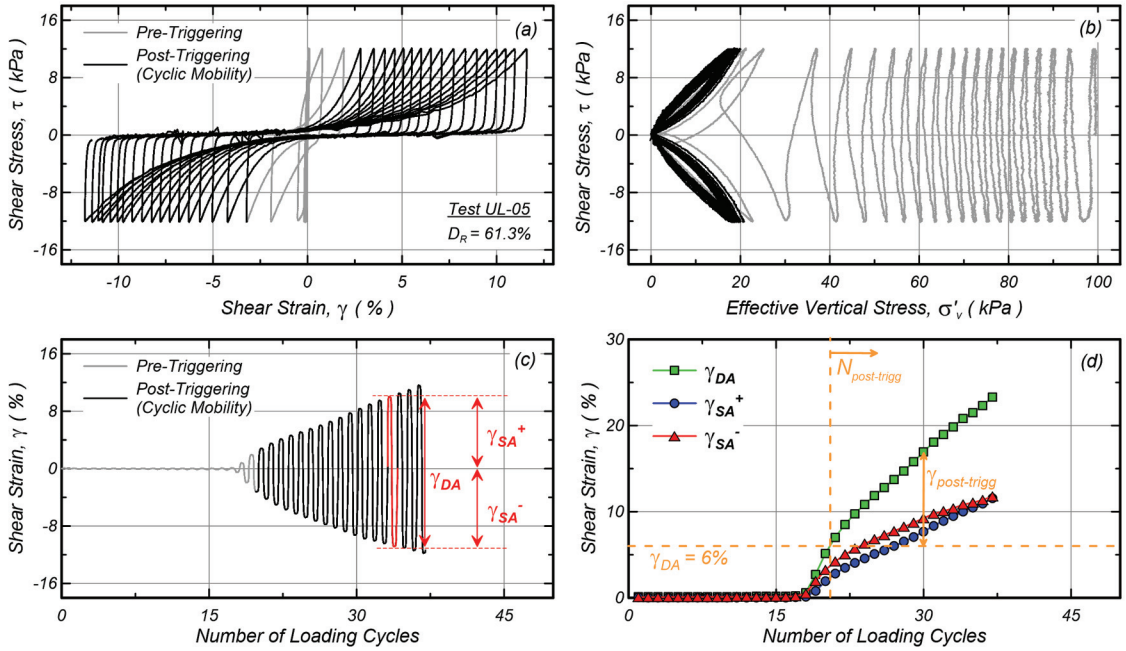

evolution of the double- and single-amplitude maximum shear strains (γ_{DA} and γ_{SA}, respectively) in each loading cycle (Figs. 1*c* and 1*d*). This approach quantifies the rate of shear strain accumulation per loading cycle or $\Delta\gamma$, which is defined by Tasiopoulou et al. (2020) as the difference in γ_{DA} or γ_{SA} between two consecutive loading cycles. Several available experimental databases (e.g., Kammerer et al. 2000; Sriskandakumar 2004) show that the post-triggering response in clean sands is characterized by an almost linear accumulation of shear strains while increasing the number of loading cycles. However, experiments performed on dense specimens of clean sands (Zhang and Wang 2012; Wichtmann and Triantafyllidis 2016) show that $\Delta\gamma$ can gradually decrease while increasing the number of post-triggering cycles, and eventually saturating at large deformations. Experiments performed to up to 50% shear strains showed that this gradual decrease of $\Delta\gamma$ can also occur on loose and medium-dense specimens (Kiyota et al. 2008; Chiaro et al. 2012, 2013), but these large deformations are not typically explored with conventional laboratory devices. For example, the hollow cylinder tests performed by Kiyota et al. (2008) on medium-dense specimens of Toyoura sand showed a progressive decrease in the rate of strain accumulation after achieving 15% shear strain. In parallel, discrete element model (DEM) simulations of cyclic undrained tests (Wang et al. 2016; Wang and Wei 2016; Wei et al. 2018) have also exhibited the gradual decrease of $\Delta\gamma$ at large strain levels. More importantly, those works have shown that the shear strain accumulation per loading cycle saturates after reaching a certain strain threshold. The gradual decrease and subsequent saturation in the shear strain accumulation observed by those works were associated with the progressive saturation of changes in the fabric of liquefied soils, as reflected by the evolution of metrics of particle-void anisotropy (Wei et al. 2018) and distances among neighboring particles (Wang et al. 2016). Despite the significant progress achieved through the aforementioned experimental and numerical efforts, the stress–strain response of sands exhibiting cyclic mobility behavior at large deformation levels remains not fully understood, and further research is needed to clarify the physics-based mechanisms (e.g., fabric evolution, dilatancy) and factors (e.g., loading conditions) controlling the post-triggering response (NASEM 2016).

The undrained cyclic response of sands largely depends on the relative density D_R and effective overburden stress σ'_{vo} (Seed and Lee 1966; Idriss and Boulanger 2008), which combined through the state or relative state parameter (Been and Jefferies 1985; Konrad 1988; Boulanger 2003) have facilitated the interpretation of sand responses within the broader framework of critical state soil mechanics. Other factors such as the grain properties (Kokusho et al. 2004), static shear bias (Sivathayalan and Ha 2011; Chiaro et al. 2012), testing device (Bhatia et al. 1985) or the initial soil fabric as determined by the sample preparation method (Vaid and Sivathayalan 2000; Sze and Yang 2014) have also been found to play a role in experimentally obtained sand responses. The effect of these factors is typically captured through frameworks that allow for the quantification of key aspects of the soil response like the pore pressure generation (e.g., Seed et al. 1976) and liquefaction triggering resistance (e.g., Seed and Lee 1966; Wijewickreme and Soysa 2016). However, few frameworks are available in the literature for quantitative evaluations of the post-triggering response and the accumulation of shear strains of sands undergoing cyclic mobility. On the basis of the almost linear accumulation of post-triggering shear strains per loading cycle observed in a large body of experimental data available in the literature, Tasiopoulou et al. (2020) quantified the rate of shear strain accumulation per loading cycle ($\Delta\gamma$) in those experiments, and found a dependency of $\Delta\gamma$ on D_R and cyclic stress amplitude τ_{cyc}. Based on that dependency, Tasiopoulou et al. (2020) proposed to quantify the shear strain accumulation through a metric called "compliance rate", defined as $\Delta\gamma$ normalized by τ_{cyc}, which physically represents the increase of compliance (i.e., inverse of stiffness) while increasing the number of post-triggering loading cycles. This framework allowed for the development of an empirical relationship of the compliance rate as

a function of D_R for five laboratory sands, which was used towards the calibration of constitutive models to capture the development of post-liquefaction deformations in system-level numerical simulations. Although this framework initially located the differences in the rate of shear strain accumulation for sands in their different grain properties, the effects of other important factors such as σ'_{vo} or the static shear bias were not studied given the limited experimental data collected from the literature.

Several efforts to provide a conclusive explanation of the fundamental mechanisms controlling the post-triggering response are available in the literature, including investigations based on empirical observations of sand behavior (Shamoto et al. 1997; Zhang et al. 1997; Zhang and Wang 2012) and results of DEM simulations (Wang et al. 2016; Wang and Wei 2016; Wei et al. 2018; Yang et al. 2021). Amongst these, Shamoto et al. (1997) provided a basis to interpret the mechanisms controlling the shear strain accumulation in undrained cyclic laboratory tests. Shamoto et al. (1997) proposed to characterize the shear strain accumulation by decoupling the shear strain component that develops during dilation (γ_d) and the shear strain component that develops at near-zero effective stress (γ_0) in each loading cycle (Fig. 2). Using this approach for torsional tests subjected to uniform and irregular cyclic loading conditions, Shamoto et al. (1997) showed that the accumulation of shear strains is governed by the development of γ_0, and that those strains are directly proportional to the maximum shear deformations achieved in the preceding loading cycle, thus hinting at the importance of previously accumulated damage in the ensuing response. The implementation of this approach on laboratory data allowed to identify that shear strains developed during dilation in each loading cycle tend to stabilize after liquefaction triggering (Zhang and Wang 2012; Humire et al. 2019). This approach has also been useful for the interpretation of DEM works aimed at finding the particle-level mechanisms controlling the development of post-triggering shear deformations. For example, the DEM results of Wang et al. (2016) and Wei et al. (2018) suggested that (*i*) the evolution of γ_d is mostly related to changes in the load-bearing stability of the grain assembly as reflected by the evolution of contact-based fabric metrics (e.g., coordination number), while (*ii*) the evolution of γ_0 is associated with changes in the particle-void distribution and distances between neighboring particles. Similar DEM analyses performed by Yang et al. (2021) suggested that the transition from γ_0 to γ_d occurs at a critical value of the coordination number, which must be reached to rebuild the load-bearing network within the grain assembly.

To better understand and characterize the post-triggering behavior of sands, this work examines the factors and mechanisms controlling the process of shear strain accumulation of clean uniform sands exhibiting cyclic mobility behavior under level-ground conditions. This is achieved by developing an extensive experimental database to characterize the post-triggering response at large shear strain levels for a broad range of different D_R values and loading conditions. First, the post-triggering response for uniform and irregular cyclic loading conditions is assessed through the evolution of γ_{DA}, with the rate of shear strain accumulation being defined as the difference in γ_{DA} between two consecutive loading cycles ($\Delta\gamma = \Delta\gamma_{DA}$). Then, the framework proposed by Tasiopoulou et al. (2020) is implemented to quantify the combined effects of relative density D_R, cyclic stress amplitude τ_{cyc}, loading device, and effective overburden stress σ'_{vo} on the rate of shear strain accumulation. Finally, and based on the approach and previous insights from Shamoto et al. (1997), a revised interpretation is provided regarding the role of strain history, τ_{cyc}, and dilation on the process of shear strain accumulation under uniform and irregular loading conditions. Tests under irregular cyclic loading conditions allow the validation of empirical observations from uniform loading tests. The results presented herein are expected to form a physics-based basis for the validation and calibration of constitutive models to capture cyclic mobility-induced deformations, as well as more broadly guide the liquefaction evaluations in geosystems comprising soils undergoing cyclic mobility.

Fig. 2. Near-zero effective stress shear strains (γ_0) and shear strains during dilation (γ_d) for a constant-volume cyclic DSS test on a dense specimen of Ottawa F-65 sand: (*a*) definition in stress–strain loop domain, (*b*) corresponding branches in stress path, and (*c*) evolution with number of loading cycles. [Color online.]

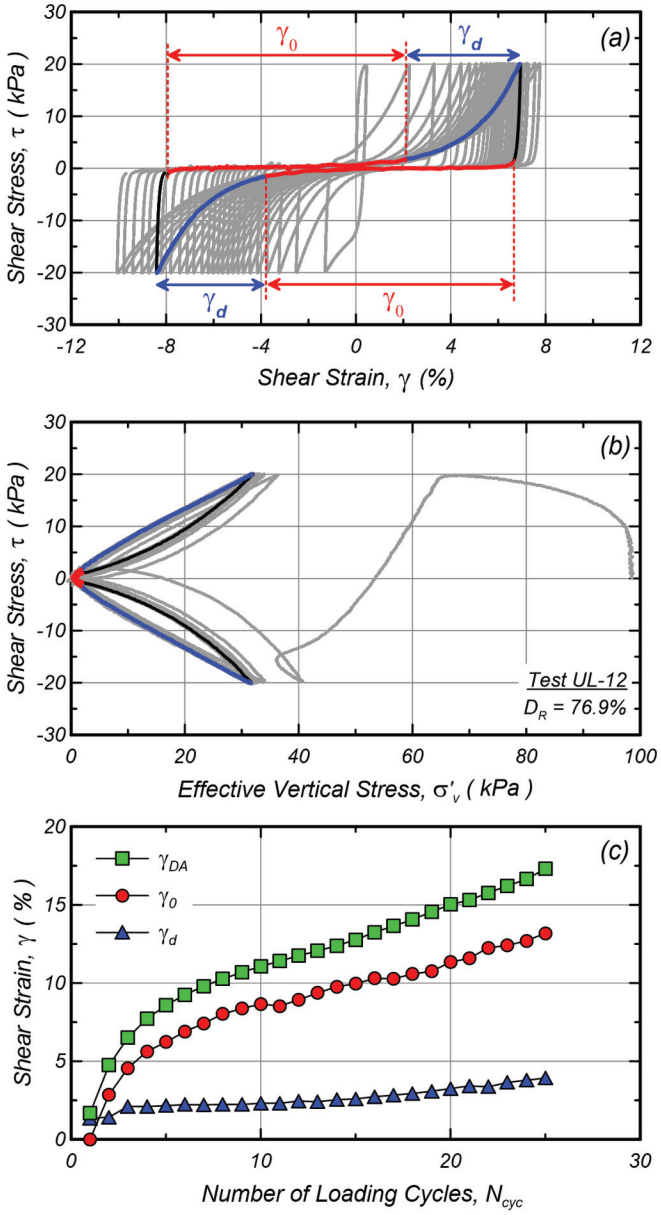

2. Experimental data

2.1. Material

Experiments were conducted on reconstituted specimens of Ottawa F-65 sand, which was the primary soil used in the Liquefaction Experiments and Analysis Projects (LEAP; Kutter et al. 2020 amongst many). In the context of the LEAP project, Ottawa F-65 sand was classified as a poorly graded sand (SP, classified in accordance with ASTM 2017), with a median grain size (D_{50}) of 0.20 mm, a coefficient of uniformity (C_u) of 1.47, a coefficient of curvature (C_c) of 0.88, and no fines (Carey et al. 2020). However, different values of minimum and maximum void ratios (e_{min} and

Table 1. Summary of constant-volume (equivalent undrained) cyclic DSS tests performed under uniform loading (UL) conditions.

Test ID	D_R (%)	σ'_{vo} (kPa)	τ_{cyc} (kPa)
UL-01	37.7	100	10
UL-02	38.7	100	10
UL-03	48.0	100	15
UL-04	59.7	100	10
UL-05	61.3	100	12
UL-06	58.7	100	15
UL-07	56.0	100	18
UL-08	63.0	100	15
UL-09	64.3	100	15
UL-10	75.2	100	15
UL-11	76.4	100	15
UL-12	76.9	100	20
UL-13	77.5	100	20
UL-14	79.0	100	20
UL-15	37.5	50	7.5
UL-16	42.1	50	7.5
UL-17	50.6	50	7.5
UL-18	56.0	50	10
UL-19	60.1	50	10
UL-20	63.4	50	7.5
UL-21	66.3	50	7
UL-22	69.6	50	8.5
UL-23	79.6	50	10
UL-24	42.3	400	60
UL-25	52.4	400	40
UL-26	55.4	400	40
UL-27	60.4	400	60
UL-28	64.9	400	34
UL-29	66.2	400	60
UL-30	70.4	400	60
UL-31	78.5	400	80

Note: D_R data correspond to values measured after consolidating at 100 kPa.

e_{max}, respectively) were reported for this material by different researchers who participated in the LEAP project and beyond (Vasko 2015; Parra Bastidas 2016; Carey et al. 2020). The variability of these parameters may be associated with the use of different laboratory methods for the determination of maximum and minimum densities, as well as with issues in the repeatability of each method (Lunne et al. 2019). Given the impact of these parameters in the evaluation of D_R, the values of e_{min} and e_{max} must be carefully selected. In this investigation, values of e_{min} and e_{max} of 0.51 and 0.78, respectively, were selected as more reliable based on the statistical analysis of the properties of Ottawa F-65 sand by Carey et al. (2020).

2.2. Testing equipment and procedures

An electromechanical dynamic cyclic simple shear (EMDCSS) device manufactured by GDS Instruments was utilized to perform constant-volume (equivalent undrained) cyclic direct simple shear (DSS) tests. The active height control system implemented in the EMDCSS device allowed constant-volume DSS tests to be performed with vertical strains below the threshold of 0.05% recommended by ASTM (2019) and below the 0.025% threshold recommended by Zekkos et al. (2018). Samples of about 70 mm in diameter and 22 mm in height were laterally enclosed within stacked Teflon-coated steel rings and a latex membrane of about 0.35 mm (±0.05 mm) in thickness. Sintered steel porous discs with protruding ridges with a height of about 1 mm were placed on the end caps to optimize shear stress transfer to the samples.

Table 2. Summary of constant-volume (equivalent undrained) cyclic DSS tests performed under irregular loading (IL) conditions.

Test ID	D_R (%)	σ'_{vo} (kPa)	$\tau_{cyc,1}$ (kPa)	$\tau_{cyc,2}$ (kPa)	$\tau_{cyc,3}$ (kPa)
IL-01	61.5	100	15	7.5	3.75
IL-02	64.4	100	15	5	10
IL-03	66.6	100	12	6	12
IL-04	68.0	100	16	8	12

Note: D_R data correspond to values measured after consolidating at 100 kPa.

Specimens were prepared with the air pluviation method, which involved raining oven-dried sand from a constant height into the soil container. For this investigation, the specimens were prepared to target post-consolidation D_R values between 37% and 80%. After applying a seating load of 10 kPa, specimens were saturated by slowly flushing deionized water from bottom to top of the specimens. Saturation was ensured by monitoring air bubbles in the outgoing water as described in Parra Bastidas (2016). Following saturation, all samples were subjected to a series of pre-conditioning strain-controlled drained cycles with an amplitude of 0.01 mm (about 0.045% shear strain) to ensure engagement of the textured top platen with the specimen (Humire et al. 2022). This pre-conditioning stage consisted of 50 drained cycles applied under a vertical stress of 100 kPa for tests with a σ'_{vo} of 100 or 400 kPa, and 115 drained cycles at a vertical stress of 25 kPa for tests with a σ'_{vo} of 50 kPa. Both pre-conditioning sequences were found to lead to similar results in terms of stress–strain response and liquefaction resistance (Humire et al. 2022). Following pre-conditioning, the vertical stress was raised to the target initial consolidation stress if the target value was larger than the vertical stress during pre-conditioning. Finally, specimens were subjected to a stress-controlled constant-volume cyclic shearing with a frequency of 0.05 Hz until a single amplitude shear strain of 10% was achieved or more than 100 loading cycles were applied in the post-triggering regime.

2.3. Testing program

The testing program comprised a series of DSS tests subjected to uniform loading conditions to evaluate the effect of cyclic stress amplitude (τ_{cyc}) and effective overburden stress (σ'_{vo}) on the process of shear strain accumulation (Table 1). Additionally, a series of experiments were performed to evaluate the effect of irregular cyclic loading conditions on the post-triggering response. Similar to the tests presented in Ziotopoulou and Boulanger (2016), irregular loading tests involved varying the τ_{cyc} along the course of the post-triggering regime in three loading stages (Table 2). The first loading stage of these tests ended after exceeding a shear strain of 4%, while the second stage ended after achieving a shear strain of 5%–7%. Results presented in this work were complemented with datasets available in the literature for the same material, which included triaxial (El Ghoraiby et al. 2017), DSS (El Ghoraiby and Manzari 2018; Morales et al. 2021; Lee et al. 2022), and hollow cylinder torsional shear tests (Ueda et al. 2020).

3. Test results and discussion

3.1. Liquefaction triggering

Before focusing on the process of shear strain accumulation, the liquefaction-triggering resistance of the experiments performed within this work were assessed to confirm expected trends on sands undergoing cyclic mobility. Considering a triggering criterion of $\gamma_{DA} = 6\%$, DSS results for relative densities around 60% were grouped to define liquefaction resistance curves for different σ'_{vo} values (Fig. 3). Results were in good agreement with (*i*) liquefaction triggering data available in the literature for the same material, (*ii*) previous works that show a decrease in the cyclic resistance when increasing σ'_{vo} (Vaid et al. 2001; Idriss and Boulanger 2008), and (*iii*) critical state theory wherein the increase of effective overburden

Fig. 3. Liquefaction triggering curves for medium-dense specimens of Ottawa F-65 sand, tested as part of this work, under varying effective overburden stresses σ'_{vo}, and comparison with available results from literature. *a* and *b* are the fitting parameters for the power law between CSR and *N*. [Color online.]

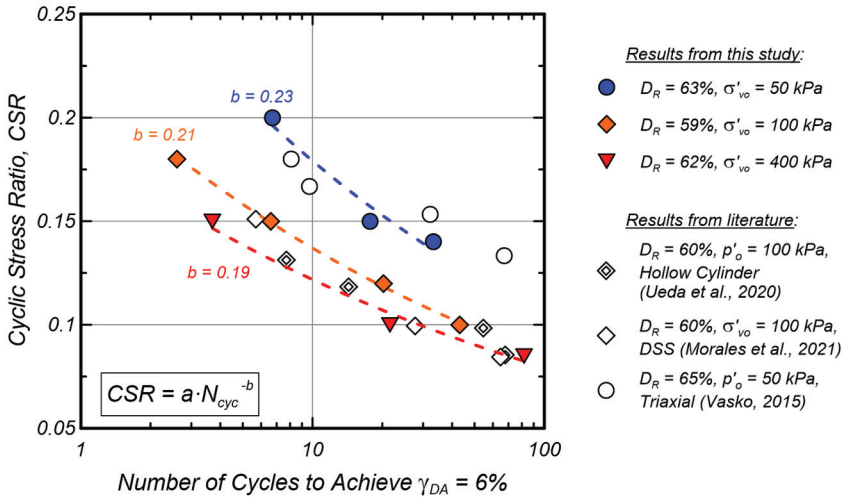

Fig. 4. Shear strain accumulation per loading cycle in (*a*) three DSS tests on medium-dense specimens, under different σ'_{vo} values but the same CSR (0.15) and similar D_R (59%–66%) values, and (*b*) three DSS tests performed on specimens with different D_R values but the same σ'_{vo} (100 kPa) and CSR (0.15). [Color online.]

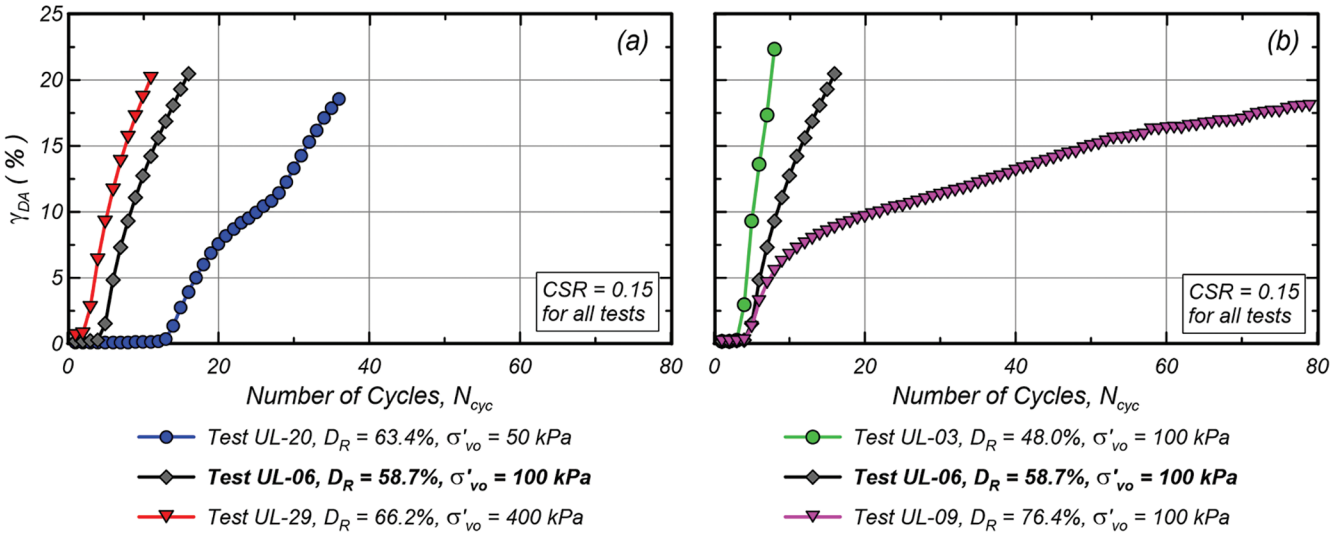

stress increases contraction and suppresses dilation, and thus reduces the overall liquefaction resistance (Vaid and Chern 1985).

3.2. Post-triggering shear strain accumulation per loading cycle

3.2.1. *Uniform loading conditions*

Figure 4 illustrates the effect of σ'_{vo} and D_R on the shear strain accumulation for a series of DSS tests sheared with the same uniform cyclic stress ratio (CSR = τ_{cyc}/σ'_{vo}). As shown in Fig. 4*a*, the shear strain accumulation per loading cycle was much faster for tests under higher σ'_{vo} values. Since the main difference between these tests was the stress level, the results confirm and strengthen the observations by Tasiopoulou et al. (2020) regarding the dependency of the rate of shear strain accumulation per loading cycle on τ_{cyc} and not on the CSR. On the contrary, the accumulation of shear strains per loading cycle was much faster for looser specimens than for denser specimens subjected to the same loading conditions (Fig. 4*b*), which confirms the strong dependency of the rate of shear strain accumulation per loading cycle on the D_R value, as shown previously by Tasiopoulou et al. (2020). Also, the accumulation of shear strains for loose and medium-dense specimens followed an almost linearly increasing trend, while for dense specimens the rate of shear strain accumulation tended to decrease gradually while increasing the number of cycles. This gradual decrease in the accumulation of strains was observed in all tests performed on dense specimens of Ottawa F-65 sand, including two tests that exhibited an almost full arrest (UL-14 and UL-23) on the rate of shear strain accumulation with no signs of having been affected by strain non-uniformities. Due to device limitations, for most of the tests presented herein, measurements of shear deformations were affected by the development of non-uniformities (e.g., rotation of confining rings) at large strain levels (γ_{DA} > 12%–18%), which can be visualized as a sudden increase in the slope of the plots of γ_{DA} versus the number of loading cycles. Therefore, it is interpreted that the gradual arrest might have occurred in looser specimens at much higher strain levels; however, that eventual gradual arrest could not be

Fig. 5. Example results of a constant-volume DSS test performed on a medium-dense specimen of Ottawa F-65 sand under irregular cyclic loading conditions, wherein the amplitude of cyclic shearing is progressively reduced over three distinct stages. [Color online.]

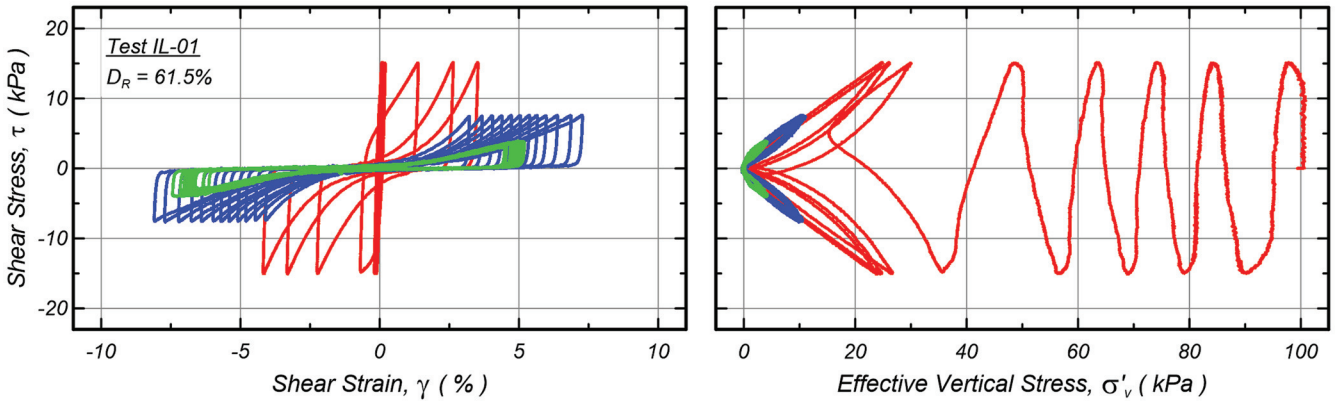

Fig. 6. Results of four DSS tests performed under irregular loading conditions, with shear strain accumulation per loading cycle, and rate of shear strain accumulation ($\Delta\gamma_{DA}$) per loading cycle shown for each test: (*a*) test IL-01, (*b*) test IL-02, (*c*) test IL-03, and (*d*) test IL-04. [Color online.]

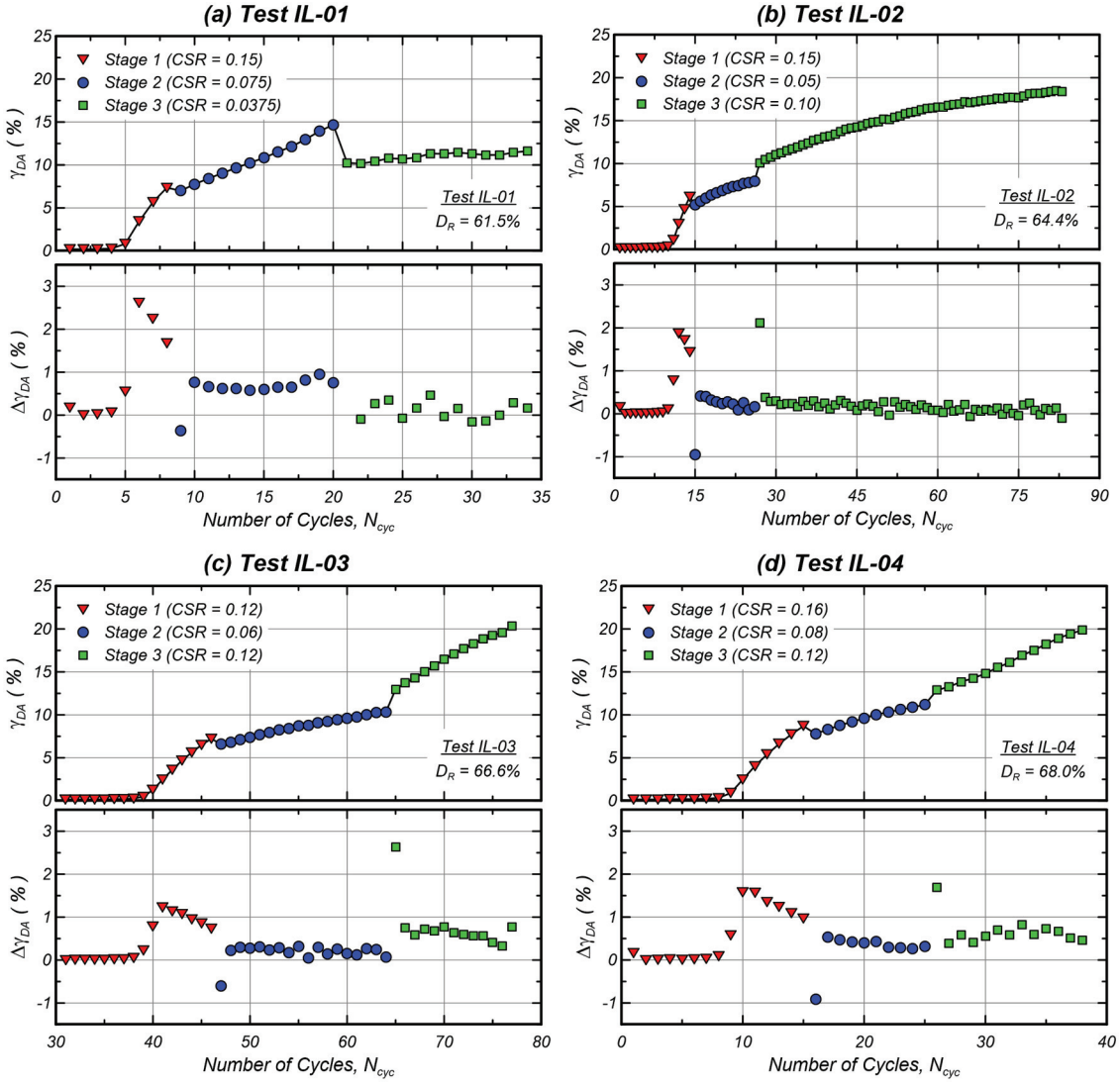

Fig. 7. Evolution of $\gamma_{post\text{-}trigg}$ per post-triggering loading cycle normalized by the cyclic stress amplitude (τ_{cyc}) in tests UL-04 to UL-07. [Color online.]

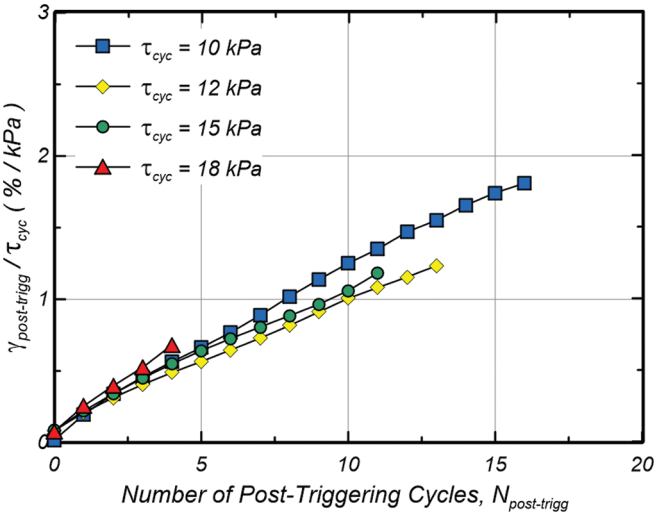

Fig. 8. Compliance rates evaluated for all DSS tests performed within this work on specimens of Ottawa F-65 sand. [Color online.]

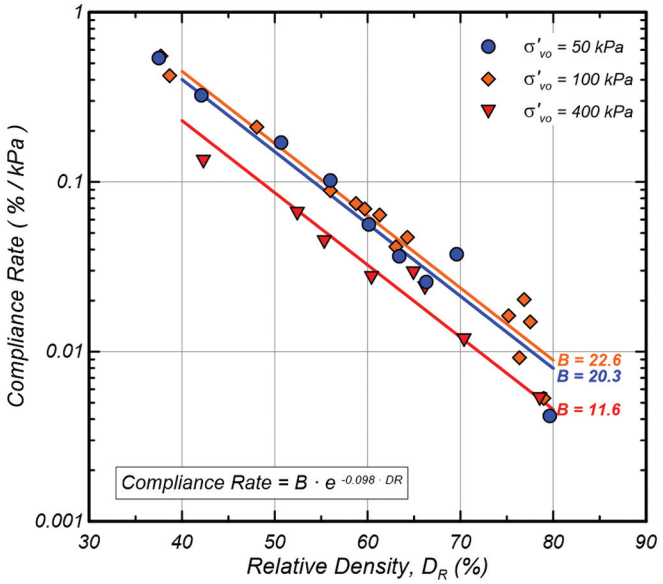

explored due to the development of non-uniform deformations at large strain levels.

3.2.2. Irregular loading conditions

Figure 5 presents an indicative stress–strain response exhibited by one of the tests conducted under irregular loading conditions, and Fig. 6 summarizes the process of shear strain accumulation exhibited by all the irregular loading DSS tests listed in Table 2. The accumulation of γ_{DA} per loading cycle for all tests was characterized by a progressively increasing trend after liquefaction triggering with evident discontinuities (drops of 1%–3% in the vertical γ_{DA} axis) when transitioning from one loading stage to another. Setting those discontinuities aside, it is evident that the rate of shear strain accumulation ($\Delta\gamma_{DA}$) varied in each stage accordingly to the changes in τ_{cyc} along the tests. For example, test IL-01 (Fig. 6*a*) showed a decrease of $\Delta\gamma_{DA}$ of about 1.5%–2.5% in the first loading stage ($\tau_{cyc,1}$ = 15 kPa) to a $\Delta\gamma_{DA}$ of about 0.6%–1.0% in the second loading stage ($\tau_{cyc,2}$ = 7.5 kPa), and later to a $\Delta\gamma_{DA}$ closer to 0 in the third loading stage ($\tau_{cyc,3}$ = 3.75 kPa). Similar observations hold for tests IL-02 to IL-04 (Figs. 6*b* to 6*d*), which showed a decrease in $\Delta\gamma_{DA}$ when transitioning from the first to the second stage ($\tau_{cyc,1} > \tau_{cyc,2}$), and then a slight increase in $\Delta\gamma_{DA}$ when passing to the third stage ($\tau_{cyc,2} < \tau_{cyc,3}$).

The shear strains obtained after transitioning from one loading stage to another suggest that the strains developed in each cycle depend on the maximum shear strain developed in the previous loading stage. For example, the first loading cycle of the second loading stage of all irregular loading tests exhibited similar shear strains to those developed in the last loading cycle of the first stage despite the reduction in τ_{cyc}. This observation is consistent with previous works that showed that the shear deformations measured in the post-triggering regime depend on the maximum deformations achieved in previous loading cycles (Shamoto et al. 1997; Zhang and Wang 2012). On the contrary, the dependency of $\Delta\gamma_{DA}$ on the τ_{cyc} on the current loading stage agrees with observations made previously for tests under uniform loading conditions (Section 3.2.1).

3.3. Factors controlling rate of shear strain accumulation

3.3.1. Compliance rate

The compliance rate defined in Tasiopoulou et al. (2020) was used to quantify the differences in the process of shear strain accumulation for different loading and testing conditions. The compliance rate was evaluated for all the experiments that were subjected to uniform loading conditions by following the procedure described by Tasiopoulou et al. (2020). First, the shear strains developed only in the post-triggering regime ($\gamma_{post\text{-}trigg}$) were isolated from the double-amplitude shear strains as illustrated in Fig. 1*d*. Then, the values of $\gamma_{post\text{-}trigg}$ were normalized by τ_{cyc} and plotted versus the number of post-triggering loading cycles ($N_{post\text{-}trigg}$) as shown in Fig. 7. The appropriateness of the normalization of the rate of shear strain accumulation with τ_{cyc} was confirmed by the good agreement of the evolution of $\gamma_{post\text{-}trigg}/\tau_{cyc}$ for tests performed with the same D_R and σ'_{vo} but different τ_{cyc}. Then, the compliance rate for each experiment was computed as half of the slope of the linear fit of the $\gamma_{post\text{-}trigg}/\tau_{cyc}$ versus $N_{post\text{-}trigg}$ curve, but only considering the data between 6% and 10% double-amplitude shear strain. This range was selected following the recommendation of Tasiopoulou et al. (2020) about defining an upper bound for the compliance rate of tests exhibiting a gradual decrease in the rate of shear strain accumulation per loading cycle. In this range, the evolution of $\gamma_{post\text{-}trigg}/\tau_{cyc}$ per loading cycle followed an almost linear trend for most of the experiments, except for two experiments performed on dense specimens ($D_R \approx 80\%$) that exhibited an early arrest on the accumulation of shear strains (tests UL-14 and UL-23).

The compliance rates obtained for all the DSS tests subjected to uniform loading conditions were plotted against D_R as shown in Fig. 8. This plot confirmed the good correlation between the compliance rate and D_R and allowed differences between the datasets with different σ'_{vo} values to be recognized. Similar to Tasiopoulou et al. (2020), power trends were fitted to each dataset using the linear least-square fitting method:

$$\text{Compliance rate} = Be^{AD_R} \quad (1)$$

where D_R corresponds to the percentage values indicated in Table 1, A was –0.098 for all datasets, while B was varied for each dataset. The coefficients of determination (R^2) of the power fits presented in Fig. 8 ranged between 0.95 and 0.97.

3.3.2. Comparison with other testing devices and procedures

Figure 9 presents a comparison between the compliance rates obtained in this work and the compliance rates obtained using

Fig. 9. Comparison of compliance rates evaluated for different experimental databases on Ottawa F-65 sand under σ'_{vo} = 100 kPa. [Color online.]

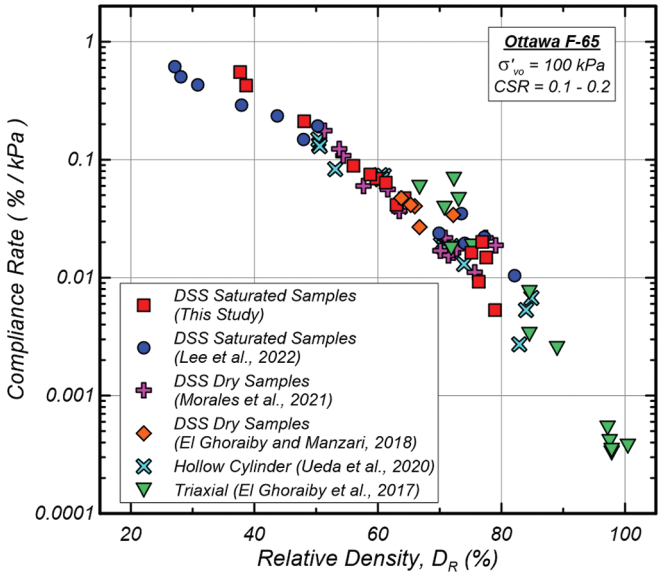

experimental data available in the literature for the same tested sand, but obtained using other testing devices and procedures. All the tests presented in Fig. 9 were performed on air-pluviated specimens of Ottawa F-65 sand that were subjected to an initial effective vertical stress of 100 kPa. For the triaxial tests performed by El Ghoraiby et al. (2017), the compliance rate was evaluated for a range of 4%–7% double-amplitude vertical strain ($\varepsilon_{v,DA}$), and shear strains were estimated as $\gamma_{DA} = 1.5\ \varepsilon_{v,DA}$. In general, good agreement was observed between the compliance rates estimated for the different experimental databases presented in Fig. 9. These results suggest that specimens prepared to the same D_R with the same sample preparation method and subjected to the same loading conditions (τ_{cyc} and σ'_{vo}) should exhibit a similar rate of shear strain accumulation per loading cycle despite differences in the mode of shearing (e.g., simple shear, torsional, triaxial). Also, almost no differences in terms of compliance rates were noticed between cyclic DSS tests performed on saturated and dry specimens, which is in agreement with previous works that have shown a negligible effect of saturation on the constant-volume response of clean sands for this type of test (Finn and Vaid 1977; Monkul et al. 2015).

3.3.3. Effect of effective overburden stress

The results presented in Fig. 8 showed that the compliance rates for the DSS tests performed with σ'_{vo} values of 50 and 100 kPa were very similar to each other. Conversely, the DSS tests performed under 400 kPa led to compliance rates smaller than those exhibited by DSS tests performed at 50 and 100 kPa. Given the normalization of the rate of shear strain accumulation by τ_{cyc} to obtain the compliance rate, its reduction while increasing σ'_{vo} is not equivalent to less strains per loading cycle with larger effective overburden stresses. To isolate and examine the effect of σ'_{vo} on the post-triggering shear strain accumulation and the compliance rate, Fig. 10 presents a comparison of the stress–strain response obtained between triggering ($\gamma_{DA} > 6\%$) and up until $\gamma_{DA} = 12\%$ for three experiments with the same D_R and loaded with the same CSR but under different σ'_{vo} values. For the test with higher σ'_{vo}, larger shear strains developed in each loading cycle, but most of those strains occurred when the soil was dilating (i.e., regaining stiffness). On the contrary, the tests with lower σ'_{vo} exhibited smaller rates of shear strain accumulation per loading cycle, but most of the shear strains occurred when the soil was at a liquefied state (i.e., near-zero stiffness). Therefore, on average, the shear strains developed in tests performed at 400 kPa occurred at higher stiffness levels than the tests at lower σ'_{vo} values, which explains the reduction of the compliance rate (i.e., inverse of stiffness). Conversely, the minimal effect of σ'_{vo} on the compliance rate when comparing tests at 50 and 100 kPa (Fig. 8) can be explained by considering that (*i*) shear strains in these tests are being controlled by strains developed at near-zero stiffness and (*ii*) the impact of friction within the testing apparatus on the development of shear strains is larger for DSS tests performed under smaller σ'_{vo} values.

3.4. Mechanisms controlling shear strain accumulation

3.4.1. Decomposition of shear strain at near-zero effective stress and at dilation

Previous DSS results under different σ'_{vo} values showed that the process of shear strain accumulation depends to a great extent on the changes in stiffness along each loading cycle. To take a closer look at this phenomenon, the approach presented by Shamoto et al. (1997) was implemented to examine the differences between shear strains developed at dilation (γ_d) and strains developed at near-zero stiffness or near-zero effective stress (γ_0) on the process of shear strain accumulation. Both strain components for all the DSS tests performed in this work were decoupled according to the procedure defined by Humire et al. (2019), and considering 2 kPa as the threshold between γ_d and γ_0. As shown previously in Fig. 2*c*, the post-triggering response was characterized by a quasi-stabilization of γ_d accompanied by a progressive increase of γ_0, which is in agreement with results presented in previous works (Zhang and Wang 2012; Humire et al. 2019). In general, γ_d exhibited a slight increase at large deformation levels (γ_{DA} >12%–18%), which was associated with the development of strain non-uniformities at those levels of deformations. These empirical observations were similar for all the DSS tests performed in this work under uniform loading conditions.

3.4.2. Role of shear strain history

To extend and further validate previous observations by Shamoto et al. (1997) regarding the dependency of γ_0 on the shear strain history, Fig. 11 summarizes and correlates the values of γ_0 for all the experiments performed under uniform loading conditions versus the γ_{DA} obtained in the respective preceding loading cycle ($\gamma_{DA,pre}$). These results confirm the linear relationship between γ_0 and $\gamma_{DA,pre}$ as shown previously by Shamoto et al. (1997). The comparison of tests on samples with different D_R values but the same σ'_{vo} shows a slightly decreasing trend of γ_0 while increasing D_R (Fig. 11*a*). On the contrary, results for different σ'_{vo} values but similar D_R values show a decreasing trend of γ_0 while increasing σ'_{vo} (Fig. 11*b*). The larger scattering of γ_0 observed for tests with a σ'_{vo} of 400 kPa is attributed to the smaller sampling used to capture the stress–strain response in the region where γ_0 is evaluated. Since all the tests were performed with a loading frequency of 0.05 Hz and sampling frequency of 500 Hz, each stress–strain loop consisted of 10 000 recording points. However, only 10 of those points were in the region where γ_0 was evaluated for tests at 400 kPa, while more than 100 points were in that region for tests at 50 and 100 kPa.

A similar relationship between γ_0 and $\gamma_{DA,pre}$ was observed for the experiments performed under irregular loading conditions. Despite the changes in τ_{cyc} amongst these tests, γ_0 and $\gamma_{DA,pre}$ presented an almost linear relationship that is similar to that exhibited by tests under uniform loading conditions with similar densities (Fig. 12). The good agreement between uniform and irregular loading tests confirms observations by Shamoto et al. (1997) regarding γ_0 being independent from τ_{cyc}, and that its value depends mostly on the shear strain history.

Fig. 10. Comparison of (*a*) stress–strain and (*b*) stress path loops obtained and isolated between liquefaction triggering and until a γ_{DA} of 12% is achieved, for three DSS tests on medium-dense sand specimens, similar CSRs, and under different effective overburden stresses (σ'_{vo} of 50, 100, and 400 kPa). [Color online.]

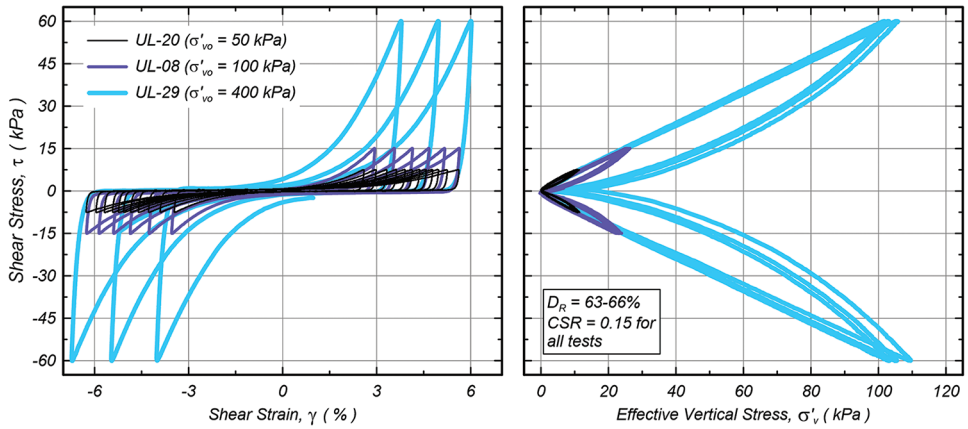

Fig. 11. Dependency of γ_0 on the γ_{DA} achieved during the preceding loading cycle ($\gamma_{DA,pre}$) for the DSS tests performed under uniform loading conditions: (*a*) comparison for different densities under σ'_{vo} = 100 kPa and (*b*) comparison for different σ'_{vo} with D_R = 55%–66%. [Color online.]

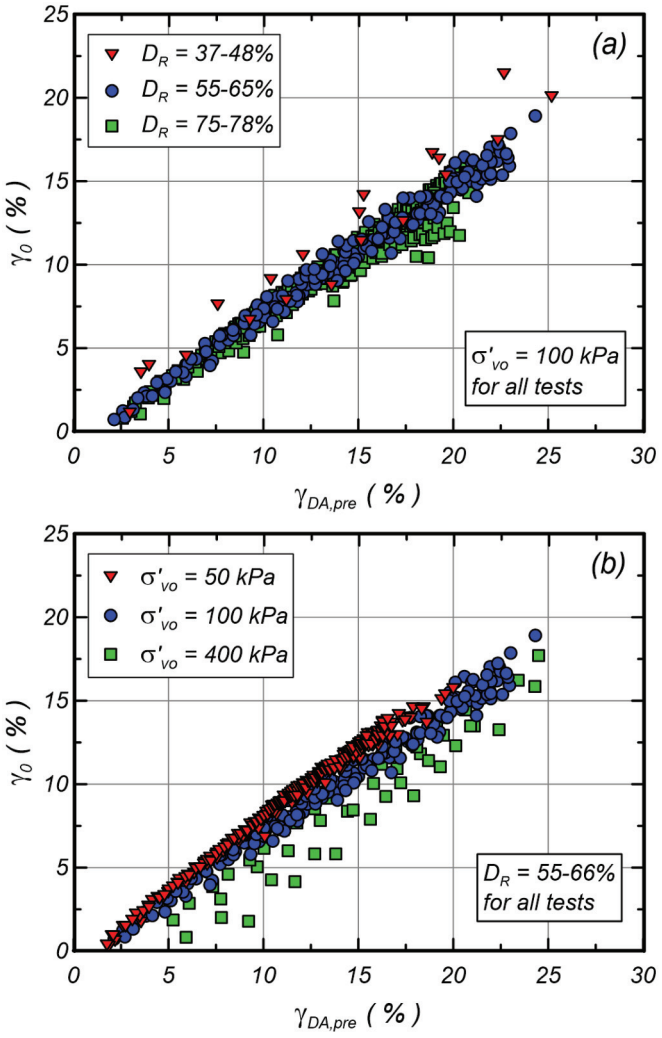

Fig. 12. Dependency of γ_0 on the γ_{DA} achieved during the preceding loading cycle ($\gamma_{DA,pre}$) for the DSS tests performed under irregular loading conditions. [Color online.]

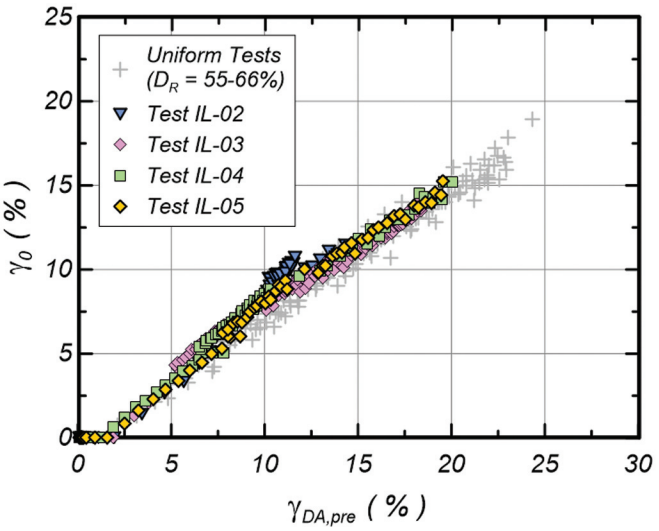

3.4.3. *Role of cyclic stress amplitude and dilation*

Previous works have concluded that the evolution of γ_d per loading cycle stabilizes towards a saturation value after liquefaction triggering (Zhang and Wang 2012; Humire et al. 2019). For the purpose of this work, the saturation values of γ_d (herein defined as γ_d^{sat}) were estimated as the average value of γ_d within a range of $\gamma_{DA,pre}$ of 6%–10%, which was the range where those strains remained almost stable. Following a rationale similar to Tasiopoulou et al. (2020) to develop the compliance rate, the values of γ_d^{sat} estimated for all the DSS tests performed under uniform loading conditions were normalized by τ_{cyc} and plotted against D_R (Fig. 13). The results show a good correlation between $\gamma_d^{sat}/\tau_{cyc}$ and D_R by following trends that are very similar to those determined for the compliance rate for different values of σ'_{vo} (Fig. 8). This suggests that the rate of shear strain accumulation per loading cycle is mostly controlled by the development of strains during dilation.

The dependency of γ_d on τ_{cyc} was also confirmed by tests conducted under irregular loading conditions, as noticed when comparing the evolution of γ_d and γ_d/τ_{cyc} per loading cycle obtained

Fig. 13. $\gamma_d^{sat}/\tau_{cyc}$ for all the experiments performed under uniform loading conditions evaluated as the average of γ_d/τ_{cyc} in the range of 6%–10% double-amplitude shear strain. [Color online.]

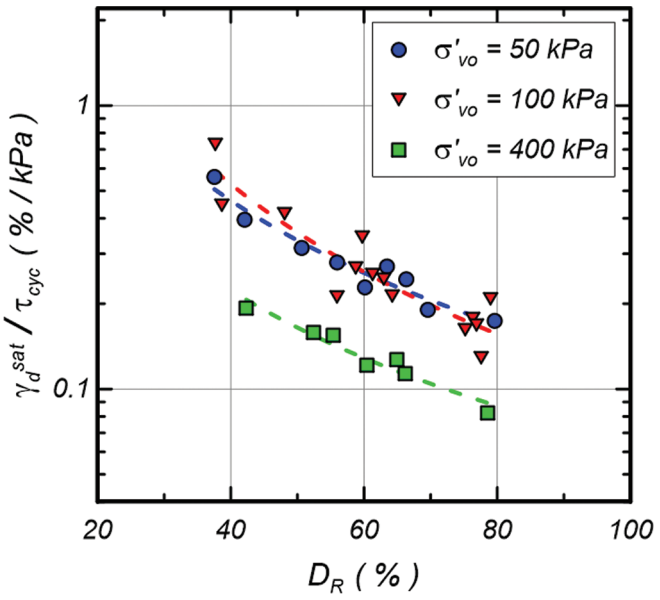

from these tests (Fig. 14). In general, the evolution of γ_d/τ_{cyc} per loading cycle followed a monotonically increasing trend that tended to stabilize around γ_d/τ_{cyc} = 0.20–0.25. However, a sudden increase in γ_d/τ_{cyc} was observed in the third loading stage of tests IL-02 to IL-04, which occurred after exceeding γ_{DA} = 12%–15% and strain non-uniformities started to affect measurements of shear deformations. More importantly, these tests exhibited a continuity in the values of γ_d/τ_{cyc} between loading stages with different CSRs, which confirms that the γ_d values developed in each loading stage are proportional to the τ_{cyc} of the current stage.

3.4.4. *Plausible explanation for gradual decrease of shear strain accumulation*

The quasi-stabilization of γ_d and the dependency of γ_0 on the strains developed in the previous half-loading cycle ($\gamma_{DA,pre}$) can explain the gradual decrease of the shear strain accumulation per loading cycle observed in tests performed on dense specimens (D_R = 65%–80%). The rationale to support this statement is explained as follows:

- Once the specimen begins to exhibit dilative behavior, γ_d increases in each loading cycle until it stabilizes to a γ_d value that remains constant with additional cycling within a few cycles after liquefaction is triggered. On the contrary, γ_0 begins to increase with continued cycling after liquefaction is triggered.
- Before the quasi-stabilization of γ_d, the values of $\Delta\gamma_{DA}$ in each cycle are defined as the sum of the increments in γ_d and γ_0 ($\Delta\gamma_{DA} \approx \Delta\gamma_d + \Delta\gamma_0$). However, once the evolution of γ_d stabilizes ($\Delta\gamma_d \approx 0$), $\Delta\gamma_{DA}$ only continues increasing due to increases in γ_0 ($\Delta\gamma_{DA} \approx \Delta\gamma_0$).
- Since $\Delta\gamma_{DA}$ decreases as cycling continues, the next increment of γ_0 decreases due to the proportionality between γ_0 and γ_{DA} (Fig. 11).
- This produces a progressive decrease in both γ_{DA} and γ_0 with cycling, which explains the gradual decrease on the rate of shear strain accumulation.

The evolution of γ_d and γ_0 described above is inherently related to changes in the soil fabric during the post-triggering regime. Following the interpretation presented in Humire et al. (2019), the quasi-stabilization of γ_d is attributed to a stabilization of changes on the particle-scale coordination number and interparticle force chains, while the evolution of γ_0 is attributed to a stabilization of changes in the particle–void distribution of the grain assembly and distances between neighboring particles. As found by Wang et al. (2016) and Wei et al. (2018), fabric metrics associated with γ_0 tend to saturate at large strain levels, which leads to a gradual arrest on the development of shear strains after achieving a certain strain threshold. This was not the case for the tests performed on loose and medium-dense specimens; however, their γ_d and γ_0 values exhibited similar dependencies to those observed in dense samples (Figs. 11*a* and 13). Therefore, it is expected that the gradual decrease in the shear strain accumulation may occur at larger strain levels for loose and medium-dense specimens. It is noted that higher shear strain levels (e.g., $\gamma > 10\%$) are difficult to investigate in a DSS device due to the increasing boundary effects at those strain levels. However, other devices such as hollow cylinder could be used to extend the findings and evaluate the applicability of the framework up to shear strains of 50% and even higher (Chiaro et al. 2013). In that sense, further work is needed to experimentally capture the cyclic mobility behavior at large strain levels across the broader spectrum of relative densities.

4. Summary and conclusions

A series of constant-volume cyclic direct simple shear (DSS) tests were performed to investigate the accumulation of shear strains in clean uniform sands undergoing cyclic mobility for a broad range of relative densities and loading conditions. In the majority of the experiments under uniform loading, the accumulation of shear strains per loading cycle was characterized by a monotonically increasing trend following initial liquefaction with an almost constant rate of shear strain accumulation in the post-triggering regime ($\gamma_{DA} > 6\%$). In experiments performed on denser specimens (D_R = 65%–80%), the rate of shear strain accumulation per loading cycle was found to be gradually decreasing. Experiments under irregular loading comprising uniform loading stages of a varying amplitude each showed that shear strains developed in each loading stage depend on (*i*) the cyclic stress amplitude τ_{cyc} of the current stage and (*ii*) the shear strains developed in previous loading stages.

The framework proposed by Tasiopoulou et al. (2020) was implemented to investigate the effect of different factors on the shear strain accumulation for tests conducted under uniform loading conditions. The results confirmed the observations of Tasiopoulou et al. (2020) regarding the dependency of the rate of post-triggering shear strain accumulation on the D_R of the specimen and τ_{cyc}. Compliance rates (i.e., rate of shear strain accumulation normalized by τ_{cyc}) evaluated in this work exhibited trends similar to those obtained from other experimental databases available in the literature for the same tested material but with other testing devices. Testing results also showed that increasing the effective overburden stress σ'_{vo} can affect the rate of shear strain accumulation, as shown by the series of tests performed under 400 kPa, which resulted in smaller compliance rates compared to those obtained under lower σ'_{vo} values (50 and 100 kPa). The decrease in compliance rate observed for tests at 400 kPa was explained by the shear strains in those tests being controlled by strains developed when the soil is dilating (i.e., regaining stiffness).

Based on the approach of Shamoto et al. (1997), the process of shear strain accumulation was characterized by decoupling the shear strains in two components: a shear strain component developed during dilation (γ_d) that tends to stabilize after liquefaction triggering and a shear strain component developed at near-zero effective stress (γ_0) that follows a monotonically increasing trend after triggering. Similar to the experimental results presented

Fig. 14. Evolution of γ_d and γ_d/τ_{cyc} per loading cycle for all the experiments under irregular loading conditions: (*a*) test IL-01, (*b*) test IL-02, (*c*) test IL-03, and (*d*) test IL-04. [Color online.]

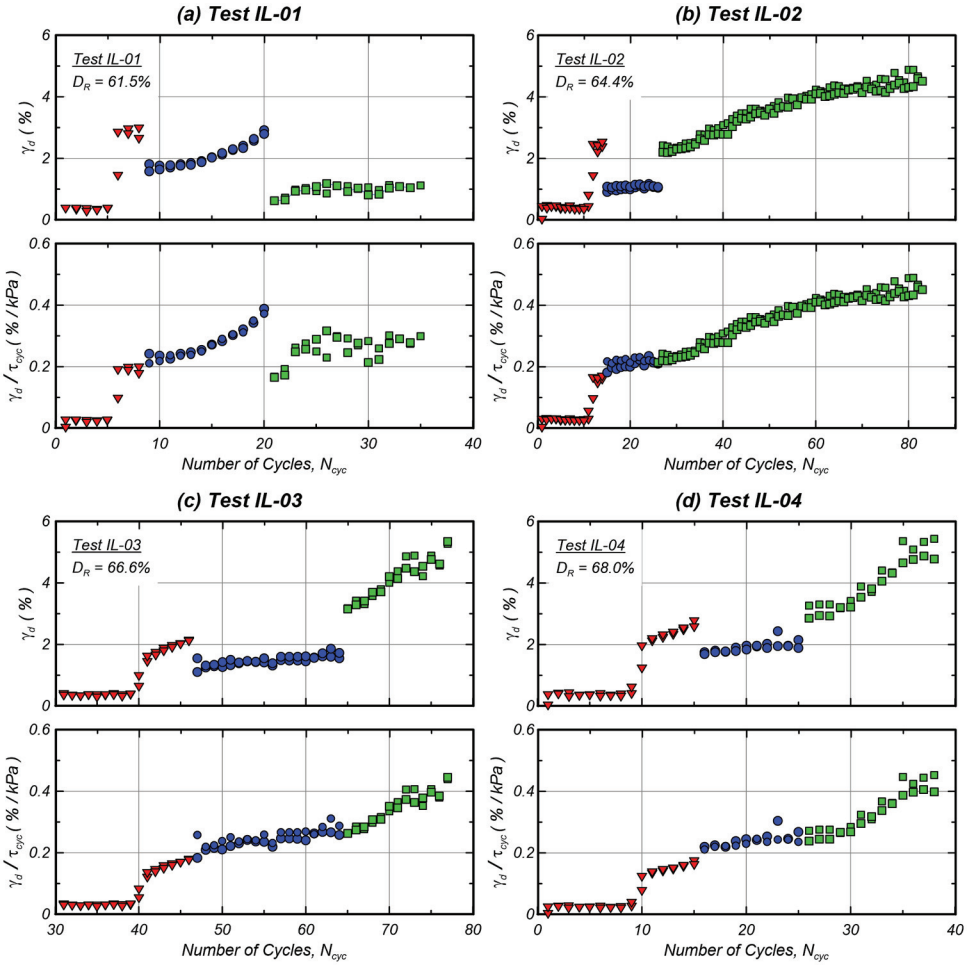

in Shamoto et al. (1997), the tests performed in this work showed that the process of shear strain accumulation is governed by the development of γ_0, whose magnitude depends on the maximum shear strain developed in the previous half-loading cycle ($\gamma_{DA,prev}$). The results also showed that γ_d depends on the cyclic stress amplitude τ_{cyc} and the relative density D_R of the specimen with similar functional dependencies to those obtained for the compliance rate. Combined, the quasi-stabilization of γ_d and the dependency of γ_0 on $\gamma_{DA,prev}$ explain the gradual decrease and eventual saturation of the rate of shear strain accumulation per loading cycle observed on dense specimens.

Results of this work experimentally confirm that, independent of relative density, the accumulation of shear strains in tests on clean sands subjected to uniform loading patterns gradually decrease after exceeding a certain strain threshold. This finding is experimentally proving the previous observations of DEM simulations of undrained cyclic tests (Wang et al. 2016; Wei et al. 2018), which have shown that the development of shear strains gradually arrests as a result of a saturation of changes of the soil fabric in the post-triggering regime and, in particular, of changes in void-based fabric metrics. Still, further investigations are needed to evaluate the extent to which this gradual decrease on the shear strain accumulation occurs in the field, and how it depends on the features of geosystems being analyzed (i.e., sloping ground conditions, spatial variability and (or) continuity of liquefiable soils). Also, further work and developments in testing devices are needed to more reliably capture large shear deformations experimentally, as the gradual decrease of the rate of shear strain accumulation and stabilization of both γ_d and γ_0 at large strain levels may be affected by the development of strain non-uniformities or other boundary effects. The use of other testing devices (e.g., hollow cylinder tests, ring shear tests) could resolve these issues and complete the picture of shear strain accumulation in the cyclic mobility regime across the broader spectrum of relative densities. Such developments will later facilitate the evaluation of the progressive arrest of the shear strain accumulation for loose and medium-dense specimens, and the formulation of relationships between saturation shear strains and other properties (e.g., state properties, grain properties).

Lastly, the results presented in this work provide a basis for the validation and calibration of constitutive models to capture cyclic mobility–induced shear strain accumulation and, therefore, to improve the estimation of liquefaction-induced deformations required for the performance-based design of geosystems. Capturing this phenomenon is particularly important for the design of geosystems at potentially liquefiable sites that can be subjected to long-duration earthquakes and, therefore, where several loading cycles can occur after liquefaction triggering. The results also highlight the need for using experimental data representative of the expected in situ soil and loading conditions given their impact on the resulting deformations, as well as the importance of prioritizing behaviors of interest given those conditions. As such, capturing the shear strains developed during dilation should be prioritized when calibrating data for high effective overburden stresses, while

capturing near-zero stiffness features should be prioritized when modeling the response under small effective overburden stresses. Even though the experimental database presented in this work already covers a broad range of conditions (e.g., relative density, effective overburden stresses, irregular loading patterns) and extends prior datasets, further research is needed to similarly quantify the effect of other factors such as initial static shear bias (i.e., sloping ground conditions) and grain properties (e.g., grain size, gradation, grain shape) on the mechanisms of shear strain accumulation.

Data availability statement

Experimental data that support the findings of this work are available from the corresponding author upon reasonable request.

Acknowledgements

The research presented in this paper was partially funded by the National Science Foundation (NSF) CMMI Award No. 1916152. Any opinions, findings, conclusions or recommendations expressed in this paper are those of the authors and do not necessarily reflect the views of NSF. The authors are grateful to Panagiota Tasiopoulou who provided thoughtful discussions that motivated the preparation of this manuscript. The authors are also grateful to Michael G. Gomez and Minyong Lee (University of Washington) for sharing their data and helping with the development of the testing procedures presented in this work.

References

ASTM. 2017. Standard practice for classification of soils for engineering purposes (Unified Soil Classification System). ASTM D2487-17. ASTM International, West Conshohocken, Pa.

ASTM. 2019. Standard test method for consolidated undrained cyclic direct simple shear test under constant volume with load control or displacement control. ASTM standard D8296-19. ASTM International, West Conshohocken, Pa.

Beaty, M., and Byrne, P.M. 1998. An effective stress model for predicting liquefaction behavior of sand. *In* Geotechnical earthquake engineering and soil dynamics III. ASCE Geotechnical Special Publication. Vol. 1. pp. 766–777.

Been, K., and Jefferies, M.G. 1985. A state parameter for sands. Géotechnique, **35**(2): 99–112. doi:10.1680/geot.1985.35.2.99.

Bhatia, S.K., Schwab, J., and Ishibashi, I. 1985. Cyclic simple shear, torsional shear and triaxial - A comparative study. *In* Advances in the art of testing soils under cyclic conditions. *Edited by* V. Khosla. ASCE, New York. pp. 232–254.

Boulanger, R.W. 2003. Relating Kα to relative state parameter index. Journal of Geotechnical and Geoenvironmental Engineering, **129**(8): 770–773. doi:10.1061/(ASCE)1090-0241(2003)129:8(770).

Boulanger, R.W., and Ziotopoulou, K. 2017. PM4Sand (version 3.1): A sand plasticity model for earthquake engineering applications. Report No. UCD/CGM-17/01. Center for Geotechnical Modeling, Department of Civil and Environmental Engineering, University of California, Davis, Calif.

Carey, T.J., Stone, N., and Kutter, B.L. 2020. Grain size analysis and maximum and minimum dry density testing of Ottawa F-65 sand for LEAP-UCD-2017. *In* Model tests and numerical simulations of liquefaction and lateral spreading. *Edited by* B.L. Kutter, M.T. Manzari, and M. Zeghal. Springer, Cham. pp. 31–44. doi:10.1007/978-3-030-22818-7.

Chiaro, G., Koseki, J., and Sato, T. 2012. Effects of initial static shear on liquefaction and large deformation properties of loose saturated Toyoura sand in undrained cyclic torsional shear tests. Soils and Foundations, **52**(3): 498–510. doi:10.1016/j.sandf.2012.05.008.

Chiaro, G., Kiyota, T., and Koseki, J. 2013. Strain localization characteristics of loose saturated Toyoura sand in undrained cyclic torsional shear tests with initial static shear. Soils and Foundations, **53**(1): 23–34. doi:10.1016/j.sandf.2012.07.016.

El Ghoraiby, M.A., and Manzari, M.T. 2018. LEAP-2018 - Stress-strain response of Ottawa F65 sand in cyclic simple shear. DesignSafe-CI, Dataset. doi:10.17603/DS2NM4W.

El Ghoraiby, M.A., Park, H., and Manzari, M.T. 2017. LEAP 2017: Soil characterization and element tests for Ottawa F65 sand. The George Washington University, Washington, D.C.

Finn, W.D.L., and Vaid, Y.P. 1977. Liquefaction potential from drained constant volume cyclic simple shear tests. *In* Proceedings of the 6th World Conference on Earthquake Engineering. New Delhi, India. pp. 2157–2162.

Humire, F., Ziotopoulou, K., Basson, M.S., and Martinez, A. 2019. Framework for tracking the accumulation of shear strains during cyclic mobility. *In* Earthquake Geotechnical Engineering for Protection and Development of Environment and Constructions - Proceedings of the 7th International Conference on Earthquake Geotechnical Engineering, (ICEGE 2019), 17–20 June 2019, Rome, Italy. *Edited by* F. Silvestri and N. Moraci. CRC Press, Taylor and Francis, London. pp. 906–2914. doi:10.1201/9780429031274.

Humire, F., Lee, M., Ziotopoulou, K., Gomez, M.G., and DeJong, J.T. 2022. Development and evaluation of pre-conditioning protocols for sand specimens in constant-volume cyclic direct simple shear tests. Geotechnical Testing Journal, **45**(3): 20210028. doi:10.1520/GTJ20210028.

Idriss, I.M., and Boulanger, R.W. 2008. Soil liquefaction during earthquakes. Monograph MNO-12. Earthquake Engineering Research Institute, Oakland, Calif.

Kammerer, A.M., Wu, J., Pestana, J.M., Riemer, M.F., and Seed, R.B. 2000. Cyclic simple shear testing of Nevada sand for PEER center project 2051999. Geotechnical Engineering Report No. UCB/GT/00-01. University of California, Berkeley, Calif.

Khosravifar, A., Elgamal, A., Lu, J., and Li, J. 2018. A 3D model for earthquake-induced liquefaction triggering and post-liquefaction response. Soil Dynamics and Earthquake Engineering, **110**: 43–52. doi:10.1016/j.soildyn.2018.04.008.

Kiyota, T., Sato, T., Koseki, J., and Abadimarand, M. 2008. Behavior of liquefied sands under extremely large strain levels in cyclic torsional shear tests. Soils and Foundations, **48**(5): 727–739. doi:10.3208/sandf.48.727.

Kokusho, T., Hara, T., and Hiraoka, R. 2004. Undrained shear strength of granular soils with different particle gradations. Journal of Geotechnical and Geoenvironmental Engineering, **130**(6): 621–629. doi:10.1061/(asce)1090-0241(2004)130:6(621).

Konrad, J.-M. 1988. Interpretation of flat plate dilatometer tests in sands in terms of the state parameter. Géotechnique, **38**(2): 263–277. doi:10.1680/geot.1988.38.2.263.

Kutter, B.L., Manzari, M.T., and Zeghal, M. 2020. Model tests and numerical simulations of liquefaction and lateral spreading LEAP-UCD-2017. Springer, Cham. doi:10.1007/978-3-030-22818-7.

Lee, M., Gomez, M.G., El Kortbawi, M., and Ziotopoulou, K. 2022. Effect of light biocementation on the liquefaction triggering and post-triggering behavior of loose sands. Journal of Geotechnical and Geoenvironmental Engineering, **148**(1): 04021170. doi:10.1061/(ASCE)GT.1943-5606.0002707.

Lunne, T., Knudsen, S., BlakerVestgården, T., Powell, J.J.M., Wallace, C.F., Krogh, L., et al. 2019. Methods used to determine maximum and minimum dry unit weights of sand: Is there a need for a new standard? Canadian Geotechnical Journal, **56**(4): 536–553. doi:10.1139/cgj-2017-0738.

Monkul, M.M., Gültekin, C., Gülver, M., Akin, Ö., and Eseller-Bayat, E. 2015. Estimation of liquefaction potential from dry and saturated sandy soils under drained constant volume cyclic simple shear loading. Soil Dynamics and Earthquake Engineering, **75**: 27–36. doi:10.1016/j.soildyn.2015.03.019.

Morales, B., Humire, F., and Ziotopoulou, K. 2021. Direct simple shear testing on Ottawa F50 and F65 sand. DesignSafe-CI, Dataset. doi:10.17603/ds2-eahz-9466.

National Academies of Sciences, Engineering, and Medicine (NASEM). 2016. State of the art and practice in the assessment of earthquake-induced soil liquefaction and its consequences. The National Academies Press, Washington, D.C. doi:10.17226/23474.

Parra Bastidas, A.M. 2016. Ottawa F-65 sand characterization. Ph.D. dissertation, University of California, Davis, Calif.

Seed, H.B., and Lee, K.L. 1966. Liquefaction of saturated sands during cyclic loading. Journal of the Soil Mechanics and Foundations Division, ASCE, **92**(6): 105–134. doi:10.1061/JSFEAQ.0000913.

Seed, H.B., Lysmer, J., and Martin, P.P. 1976. Pore-water pressure changes during soil liquefaction. Journal of the Geotechnical Engineering Division, ASCE, **102**(4): 323–346. doi:10.1061/AJGEB6.0000258.

Shamoto, Y., Zhang, J.-M., and Goto, S. 1997. Mechanism of large post-liquefaction deformation in saturated sand. Soils and Foundations, **37**(2): 71–80. doi:10.3208/sandf.37.2_71.

Sivathayalan, S., and Ha, D. 2011. Effect of static shear stress on the cyclic resistance of sands in simple shear loading. Canadian Geotechnical Journal, **48**(10): 1471–1484. doi:10.1139/t11-056.

Sriskandakumar, S. 2004. Cyclic loading response of Fraser River sand for validation of numerical models simulating centrifuge tests. M.Sc. thesis, Department of Civil Engineering, University of British Columbia.

Sze, H.Y., and Yang, J. 2014. Failure modes of sand in undrained cyclic loading: Impact of sample preparation. Journal of Geotechnical and Geoenvironmental Engineering, **140**(1): 152–169. doi:10.1061/(asce)gt.1943-5606.0000971.

Tasiopoulou, P., Ziotopoulou, K., Humire, F., Giannakou, A., Chacko, J., and Travasarou, T. 2020. Development and implementation of semiempirical framework for modeling postliquefaction shear deformation accumulation in sands. Journal of Geotechnical and Geoenvironmental Engineering, **146**(1): 04019120. doi:10.1061/(ASCE)GT.1943-5606.0002179.

Ueda, K., Uemura, K., and Vargas, R.R. 2020. Data for: Dynamic torsional hollow-cylinder shear tests of Ottawa F-65 sand. Mendeley Data, V1. doi:10.17632/gv78bymth9.1.

Vaid, Y.P., and Chern, J.C. 1985. Cyclic and monotonic undrained response of saturated sands. *In* Advances in the art of testing soils under cyclic conditions. *Edited by* V. Khosla. ASCE, New York. pp. 120–147.

Vaid, Y.P., and Sivathayalan, S. 2000. Fundamental factors affecting liquefaction susceptibility of sands. Canadian Geotechnical Journal, **37**(3): 592–606. doi:10.1139/t00-040.

Vaid, J.P., Stedman, J.D., and Sivathayalan, S. 2001. Confining stress and static shear effects in cyclic liquefaction. Canadian Geotechnical Journal, **38**(3): 580–591. doi:10.1139/t00-120.

Vasko, A. 2015. An investigation into the behavior of Ottawa sand through monotonic and cyclic shear tests. M.Sc. thesis, The George Washington University, Washington, D.C.

Wang, G., and Wei, J. 2016. Microstructure evolution of granular soils in cyclic mobility and post-liquefaction process. Granular Matter, **18**: 51. doi:10.1007/s10035-016-0621-5.

Wang, R., Fu, P., Zhang, J.M., and Dafalias, Y.F. 2016. DEM study of fabric features governing undrained post-liquefaction shear deformation of sand. Acta Geotechnica, **11**(6): 1321–1337. doi:10.1007/s11440-016-0499-8.

Wei, J., Huang, D., and Wang, G. 2018. Microscale descriptors for particle-void distribution and jamming transition in pre- and post-liquefaction of granular soils. Journal of Engineering Mechanics, **144**(8): 04018067. doi:10.1061/(ASCE)EM.1943-7889.0001482.

Wichtmann, T., and Triantafyllidis, T. 2016. An experimental database for the development, calibration and verification of constitutive models for sand with focus to cyclic loading: part I—tests with monotonic loading and stress cycles. Acta Geotechnica, **11**(4): 739–761. doi:10.1007/s11440-015-0402-z.

Wijewickreme, D., and Soysa, A. 2016. Stress-strain pattern-based criterion to assess cyclic shear resistance of soil from laboratory element tests. Canadian Geotechnical Journal, **53**(9): 1460–1473. doi:10.1139/cgj-2015-0499.

Yang, M., Taiebat, M., Mutabaruka, P., and Radjaï, F. 2021. Evolution of granular materials under isochoric cyclic simple shearing. Physical Review E, **103**(3): 032904. doi:10.1103/PhysRevE.103.032904.

Zekkos, D., Athanasopoulos-Zekkos, A., Hubler, J., Fei, X., Zehtab, K.H., and Allen Marr, W. 2018. Development of a large-size cyclic direct simple shear device for characterization of ground materials with oversized particles. Geotechnical Testing Journal, **41**(2): 263–279. doi:10.1520/GTJ20160271.

Zhang, J.-M., and Wang, G. 2012. Large post-liquefaction deformation of sand, part I: physical mechanism, constitutive description and numerical algorithm. Acta Geotechnica, **7**(2): 69–113. doi:10.1007/s11440-011-0150-7.

Zhang, J.-M., Shamoto, Y., and Tokimatsu, K. 1997. Moving critical and phase-transformation stress state lines of saturated sand during undrained cyclic shear. Soils and Foundations, **37**(2): 51–59. doi:10.3208/sandf.37.2_51.

Ziotopoulou, K., and Boulanger, R.W. 2016. Plasticity modeling of liquefaction effects under sloping ground and irregular cyclic loading conditions. Soil Dynamics and Earthquake Engineering, **84**: 269–283. doi:10.1016/J.SOILDYN.2016.02.013.